JOURNAL OF THE ROYAL SOCIETY Interface

J. R. Soc. Interface (2008) **5**, 845–853
doi:10.1098/rsif.2007.1309
Published online 22 January 2008

Sliding-induced adhesion of stiff polymer microfibre arrays. II. Microscale behaviour

Bryan Schubert[1,*], Jongho Lee[2], Carmel Majidi[1] and Ronald S. Fearing[1]

[1]*Department of Electrical Engineering and Computer Sciences, and* [2]*Department of Mechanical Engineering, University of California, Berkeley, CA 94720, USA*

The adhesive pads of geckos provide control of normal adhesive force by controlling the applied shear force. This frictional adhesion effect is one of the key principles used for rapid detachment in animals running up vertical surfaces. We developed polypropylene microfibre arrays composed of vertical, 0.3 μm radius fibres with elastic modulus of 1 GPa which show this effect for the first time using a stiff polymer. In the absence of shear forces, these fibres show minimal normal adhesion. However, sliding parallel to the substrate with a spherical probe produces a frictional adhesion effect which is not seen in the flat control. A cantilever model for the fibres and the spherical probe indicates a strong dependence on the initial fibre angle. A novel feature of the microfibre arrays is that adhesion improves with use. Repeated shearing of fibres temporarily increases maximum shear and pull-off forces.

Keywords: bio-inspired adhesion; gecko; frictional adhesion; shear

1. INTRODUCTION

The gecko is well known to be excellent at scaling vertical surfaces and even clinging inverted to ceilings. However, these abilities are not the result of exceptional peel force, which can be found in standard pressure-sensitive adhesives, but instead are derived from clever use of moderate normal adhesion controlled by shear forces, termed *frictional adhesion* (Autumn *et al.* 2006*b*). Frictional adhesion allows geckos to control the magnitude of normal adhesion through the application of shear force. This lets them easily engage and disengage their adhesive pads (Gravish *et al.* 2008).

In frictional adhesion, a contact under tension is only maintained if the tensile contact force is at an angle less than α with respect to a surface, as shown for a single setal stalk (Autumn *et al.* 2000). Specifically, the angle α defines a relationship between force tangential to the surface, the shear force F_t, and force normal to the surface, F_n:

$$F_t \geq -\frac{F_n}{\tan \alpha}. \tag{1.1}$$

This equation shows the minimum shear force necessary to withstand a given tensile force. Frictional adhesion has been shown in Tokay geckos by dragging setal arrays with their natural curvature as shown in figure 1*a*. During loading, there may be slip since the setal shafts are free to rotate in order to conform to the surface. Therefore, the dot-dashed line demarcating Coulomb friction in figure 1*b* provides a bound on the value of shear force that can be observed given compressive loading. During pull-off, the dotted line in figure 1*b* marks the frictional adhesion angle α that is shown to be approximately 30° (Autumn *et al.* 2006*b*).

Frictional adhesion has recently been demonstrated in synthetic structures with large angled stalks (380 μm base width) made out of soft polymer (0.3 MPa; Santos *et al.* 2007), and 9.5 μm radius by 100 μm long stalks using 2.9 MPa spatular tips (Murphy *et al.* 2007). Interestingly, Varenberg & Gorb (2007) have shown an opposite effect using soft polymer stalks (3 MPa) with mushroom-shaped spatulae. In these mushroom-shaped structures, large shear forces rotate the tips reducing contact area and hence normal pull-off force. In this paper, we consider a stiffer polymer material (1 GPa). Stiff polymers are more durable and possibly easier to make self-cleaning.

Adhesion properties for gecko-inspired synthetic adhesives can be understood by modelling the setae as angled cantilever beams (Sitti & Fearing 2003; Gao *et al.* 2005; Spolenak *et al.* 2005; Autumn *et al.* 2006*a*; Gravish *et al.* 2008). Naturally angled cantilever beams show greater compliance in the normal direction than vertical fibres, which must undergo buckling in order to conform to a surface (Autumn *et al.* 2006*a*; Majidi *et al.* 2006). However, when a shear force is applied to the tip of a vertical beam, it becomes effectively angled, increasing normal compliance and allowing more conformal contact of the array and surface. It follows that the application of shear also aids compliance of angled cantilever beams (Autumn *et al.* 2006*a*). This is an important property evolved by the gecko to reduce the effective modulus of its stiff fibre arrays (E=1.5 GPa; Peattie *et al.* 2007) to within the Dahlquist criterion for tack (E<100 kPa at room temperature and 1 Hz; Autumn *et al.* 2006*a*). The angling of setal fibres

*Author for correspondence (bschuber@eecs.berkeley.edu).

Electronic supplementary material is available at http://dx.doi.org/10.1098/rsif.2007.1309 or via http://journals.royalsociety.org.

Received 18 November 2007
Accepted 2 January 2008

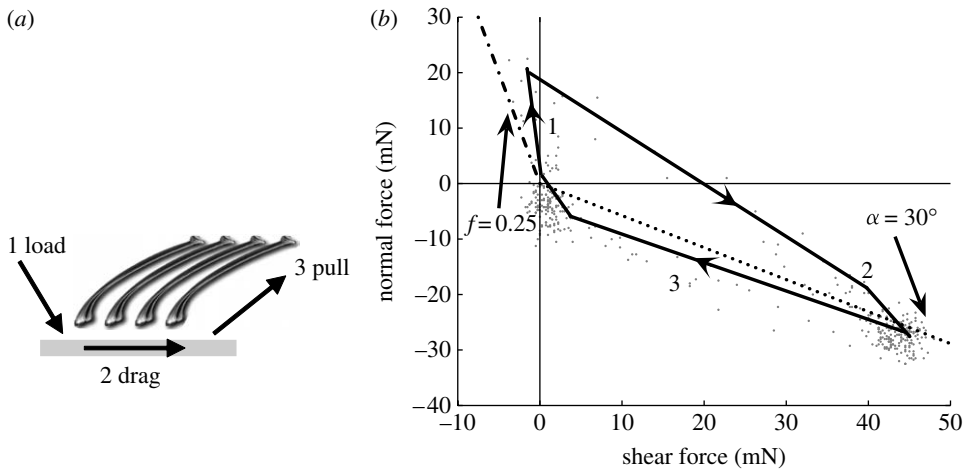

Figure 1. (*a*) Loading path of natural gecko setae. Arrows represent the motion of the setal shafts with respect to the surface. (*b*) Normal force, F_n, versus shear force, F_t, for a LDP experiment with the curvature of gecko setal shafts. Loading path starts near the origin. The Coulomb (dot-dashed line) friction with friction coefficient $f = 0.25$, and frictional adhesion (dotted line) with $\alpha = 30°$. Data adapted with permission from Autumn *et al.* (2006*b*).

combined with uncurling of spatular tips is a probable mechanism for frictional adhesion in the gecko.

In this paper, we show frictional adhesion with stiff ($E = 1$ GPa) polymer microfibres, through load–drag–pull (LDP) experiments similar to those used on gecko setal arrays (Autumn *et al.* 2006*b*). The arrays, shown in figure 2, consist of initially vertical polypropylene fibres of length 17–20 μm (owing to fibre length variation) and radius 0.3 μm, with density of 42×10^6 cm^{-2}. The repeated measurements reveal that the fibre array performance does not decrease even after more than 100 LDP trials. In fact, their shear force and normal adhesion increase with use, and they develop slight directionality properties. We show that the observed frictional adhesion behaviour during pull-off is consistent with a cantilever model for the fibres.

This paper examines the behaviour of fixed patches of these fibres in small isolated regions less than 0.1 cm in diameter, using a spherical probe and light loading. By fixing the patch to a compliant substrate, normal adhesive forces can be sustained. In contrast, part I of this paper (Lee *et al.* 2008) examines the behaviour of a free patch contacting a flat surface, which has an area (4 cm^2) more than 400 times larger than spherically probed regions. Although the free patch cannot sustain normal adhesion, the flat geometry and compliant backing used in Lee *et al.* (2008) can sustain estimated fibre shear forces 20 times greater than those used in spherical probe tests. The two parts of this paper show that sliding-induced adhesion is obtained for both micro- and macroscale contacts.

2. MATERIAL AND METHODS

2.1. Material preparation

Samples were fabricated by casting a single layer of 25 μm thick polypropylene (TF-225-4, Premier Lab Supply, Inc., Port St Lucie, FL, USA) in a vacuum oven at 200°C into a 20 μm thick polycarbonate filter (Isopore, Millipore, Inc., Billerica, MA, USA) containing 0.6 μm diameter pores. The polycarbonate filter was etched in methylene chloride, and resulting samples were rinsed in isopropyl alcohol and air-dried. Flat control samples were produced by processing the 25 μm thick polypropylene film as above except without the use of the filter.

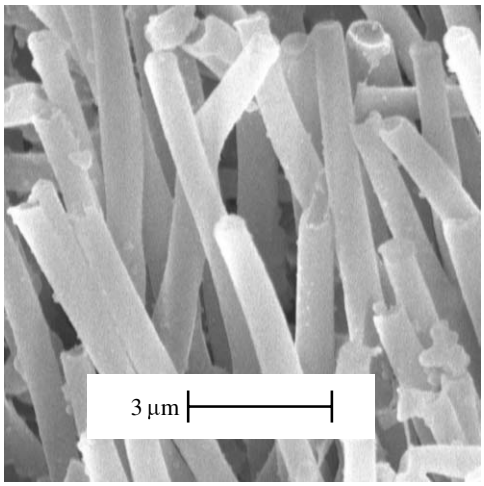

Figure 2. A scanning electron microscope (SEM) image showing shape of tips of synthetic microfibres ($l = 20$ μm and $r = 0.3$ μm).

The specific aspect ratio of the fibres was chosen to maximize fibre density while avoiding clumping for this particular moulding process (Schubert *et al.* 2007). The moulding process produces fibres that are naturally vertical, and therefore show poor adhesion from pure normal loading, which is similar to the non-adhesive default state exhibited by the gecko (Autumn & Hansen 2006). An adhesive force from pure normal loading can be achieved with permanently angled fibres (Aksak *et al.* 2007; Murphy *et al.* 2007), but naturally vertical fibres have the interesting property of shear activation, allowing the normal adhesive force to be switched on and switched-off. This effect is important for quick engagement and release of adhesive pads.

2.2. Measurement methods

Small contact regions (approx. 0.01 cm^2) were probed with a spherical indenter to measure simultaneous normal and shear forces while minimizing alignment

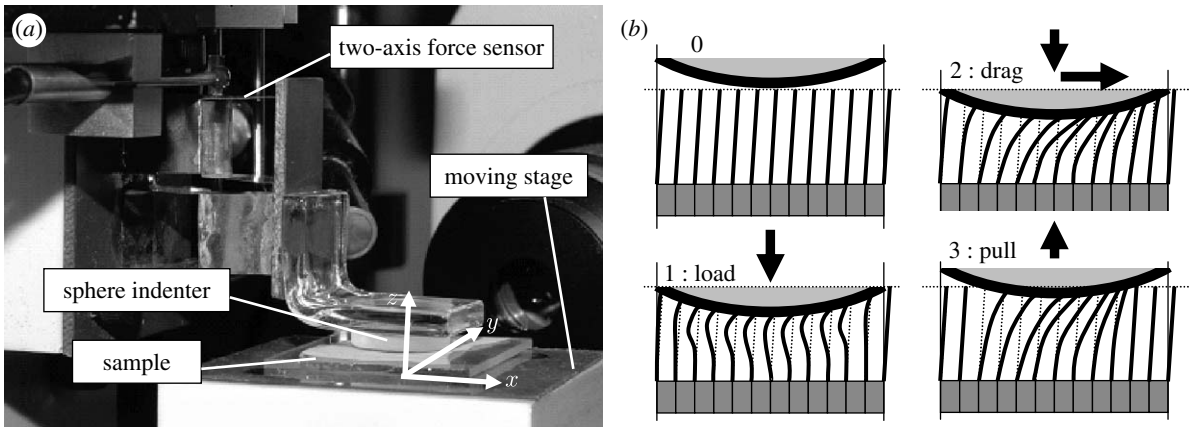

Figure 3. (*a*) Two-axis milliscale normal and shear force sensor. (*b*) Path of the probe during LDP test with estimated fibre behaviour.

issues, such as coplanarity. The small contact area allowed examination of regions of interest while avoiding damaged or defective areas. The spherical indenter also approximates contact with a single asperity, where fibres are in both compression and tension.

Deflections of the probe were measured by a two-axis force sensor (Schubert *et al.* 2007). The force sensor uses a spherical lens ($R=5.17$ cm), four double cantilevers (stiffness in z-axis, 820 N m^{-1} and y-axis, 1100 N m^{-1}), two optical probes (MTI-2100 with MTI-2062E; MTI Instruments, Albany, NY, USA; 44 nm resolution at 1 kHz, 190 µm range), and a nanopositioning stage (P-611 Nanocube, Physik Instrumente, Irvine, CA, USA; 10 nm resolution, 100 µm range) as shown in figure 3*a*. The total resolution and range of the system is 36 µN–156 mN in the z-direction and 48 µN–209 mN in the y-direction. Each sample was fixed on the nanopositioning stage using Gel-Pak (Gel-Pak, Hayward, CA, USA), and the stage was driven in the y- and z-directions (see figure 3*a*) for indentation and LDP experiments. Before testing, the spherical probe was cleaned with isopropanol.

Indentation experiments measure the normal and tangential forces that result from loading and unloading a sample only in the normal direction (z-direction). In these experiments, the probe indented the sample until a specified compressive force was reached (0.5 or 2.0 mN), then the probe retracted until no force was measured. LDP experiments measure combined shear and normal adhesion forces of the patches (Autumn *et al.* 2006*b*). In these experiments, the samples were loaded in the z-direction until a prescribed normal force was reached (0.5 or 2.0 mN), then the samples were displaced tangentially (y-direction) and, finally, they were unloaded in the z-direction as shown in figure 3*b*. The tangential displacement for experiments was 60 µm unless stated otherwise. This distance captures the interesting behaviour of the fibres (see §3; electronic supplementary material). For most experiments, normal loading, shearing and normal pull-off were performed at 10 µm s^{-1} for both the indentation and LDP experiments. This speed was chosen to stay within the range of other LDP experiments on synthetic (Murphy *et al.* 2007) and natural gecko fibre arrays (Autumn *et al.* 2006*b*).

3. RESULTS

Similarly to Lee *et al.* (2008), LDP tests demonstrated increasing shear forces during sliding. While Lee *et al.* (2008) showed low peel strength (0.15 N m^{-1}) on the whole patch, here a frictional adhesion effect was observed during normal pull-off with a spherical probe, whereby the normal tensile force was proportional to shear force. Repeated LDP testing showed that fibre arrays continue to function after more than 100 experiments, and they gain shear force and pull-off force with each trial.

3.1. LDP with spherical probe

LDP experiments were conducted on a fibre array and smooth control as shown in figure 4*a*,*b*. Figure 4*a* shows that the shear force rises dramatically while the probe is being dragged across the sample (between points 1 and 2). For Coulomb friction ($F_t=fF_n$), this would correspond to a coefficient of friction $f>10$, as shown previously in Majidi *et al.* (2006). In contrast, experiments on the control in figure 4*b* show a relatively low shear force, and a coefficient of friction $f=0.2$, typical of a stiff polymer on glass.

Figure 4*c* is a plot of a pure normal indentation without sliding on a fibrillar sample. This figure shows that without shearing the fibres there is no measurable normal adhesion. Figure 4*d* takes the data from figure 4*a*–*c* and plots them in force space, to more clearly show the frictional adhesion properties of the fibre arrays. Initially, the normal and shear forces stay within the conventional Coulomb friction cone, and the probe indents approximately 4 µm in the z-direction. When dragging begins at point 1, the normal force falls and the shear force rises quickly showing that the fibres are bending into a more compliant configuration. After moving 60 µm in the y-direction, the probe is pulled away at point 2 and the normal adhesion is evident while the shear force persists. The retraction is bounded by a frictional adhesion angle of approximately $\alpha=22°$, and the maximum pull-off force occurs at an indentation depth of 2 µm. Although the reported indentation depths are not explicitly shown in figure 4, they can be estimated from the probe speed of 10 µm s^{-1}.

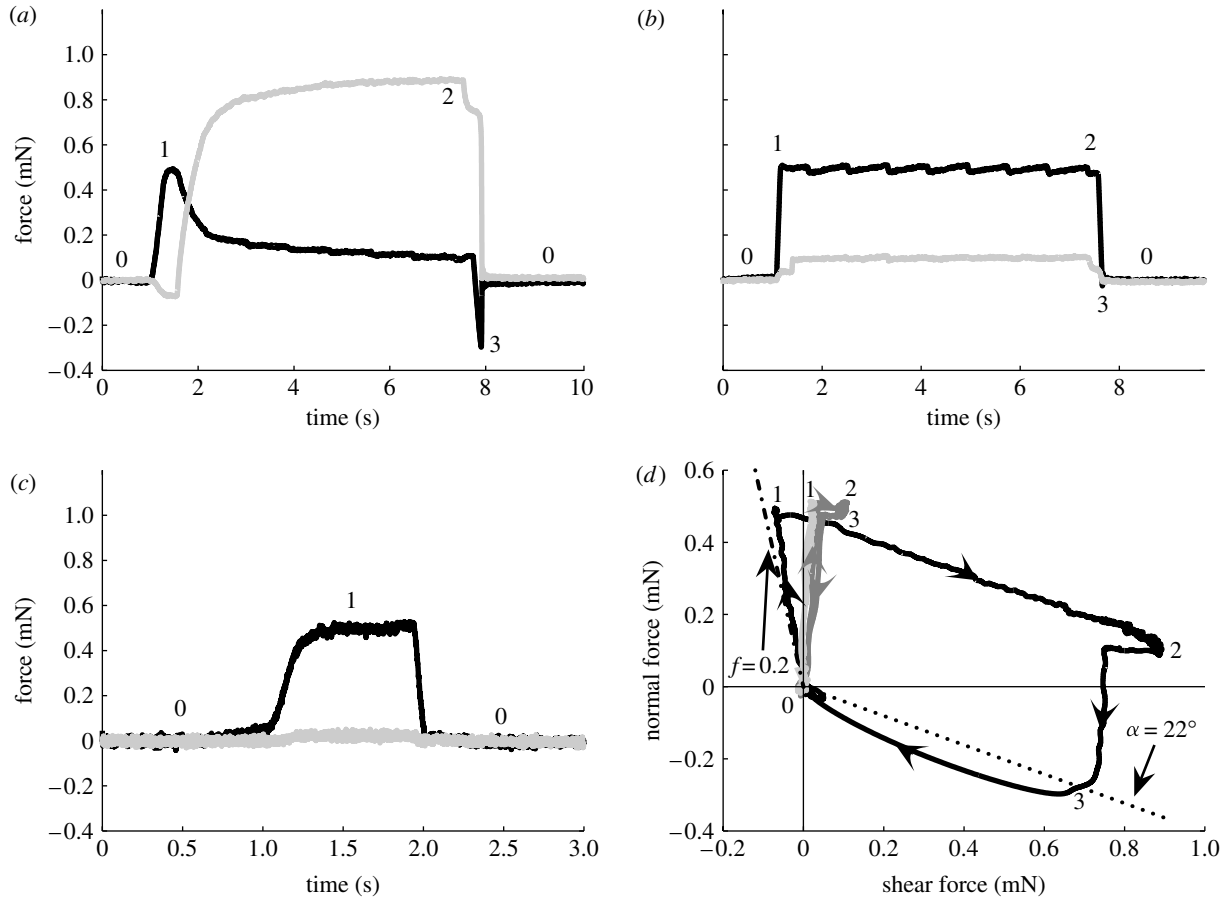

Figure 4. LDP tests with a spherical probe on (*a*) fibrillated patch and (*b*) smooth polypropylene control. (*c*) Normal indentation and pull-off without drag (load/pull) on fibrillated patch shows unmeasurable adhesion. (*d*) Plots (*a*–*c*) in force space clearly demonstrate frictional adhesion. The Coulomb friction (dot-dashed line) with $f = 0.2$, and frictional adhesion (dotted line) with $\alpha = 22°$ (black line, fibrillar; dark grey line, smooth; light grey line, load/pull). Numbers along curves correspond to the loading stages shown in figure 3*b*. Probe speed is 10 μm s^{-1}. (*a*–*c*) Black line, normal force; grey line, shear force.

In tests on the natural setal arrays (Autumn *et al.* 2006*b*), frictional adhesion is exhibited during the drag phase, as well as the pull phase. This is because the natural setae pull into tension while dragging. In contrast, this effect is not seen in the LDP experiments shown in figure 4 possibly owing to the spherical probe geometry, which causes some fibres to be in compression while others are in tension (see §4). The lack of a spatula is also probably a factor because structures with spatulae, such as those in Murphy *et al.* (2007), show tension developed during sliding. To demonstrate sliding with tensile load, the balance of tensile and compressive fibres can be shifted by retracting the probe slightly during the drag phase. Figure 5 shows the results of performing a retraction of 1 μm during the drag phase (point 2.5). The fibrillar patches lose some shear force because the net normal force is now tensile, but, as expected, the flat control sample loses contact completely. The force space plot in figure 5*d* has a similar shape to that in figure 4*d*, so it is reasonable to extract frictional adhesion information from either set of data.

In many adhesive materials, viscoelastic dissipative effects are significant. The LDP tests were repeated with sliding velocities between 5 and 100 μm s^{-1}, and as shown in figure 6, no major differences were observed. The lack of velocity dependence for these polypropylene microfibre arrays is discussed further in Lee *et al.* (2008), and shown for the whole patch in the range from 48 to 240 μm s^{-1}.

Figure 3*b* depicts the fibres being buckled slightly in step 1 due to the normal indentation of the probe. Owing to this loading, it takes a short sliding distance to orient and engage the fibres. Figure 7 shows the normal and shear forces for LDP experiments with tangential displacements of 2, 20 and 60 μm. These plots show that the shear force builds steadily over approximately 20 μm of displacement, while the normal force drops off until both the forces plateau. This effect is indicative of the fibres bending over until they reach an equilibrium sliding configuration. As predicted by frictional adhesion (equation (1.1)), the magnitude of the pull-off force grows as the shear force builds from sliding. More complete data for 0.5 and 2.0 mN preload values can be found in the electronic supplementary material.

3.2. Repeated LDP tests

To test durability and repeatability, over 100 LDP experiments were performed on five different fibre patches and two separate controls. Interestingly, repeated LDP tests have the effect of increasing shear and pull-off forces. Figure 8 shows the first and the 146th shear experiment on a fibre array. Prior to

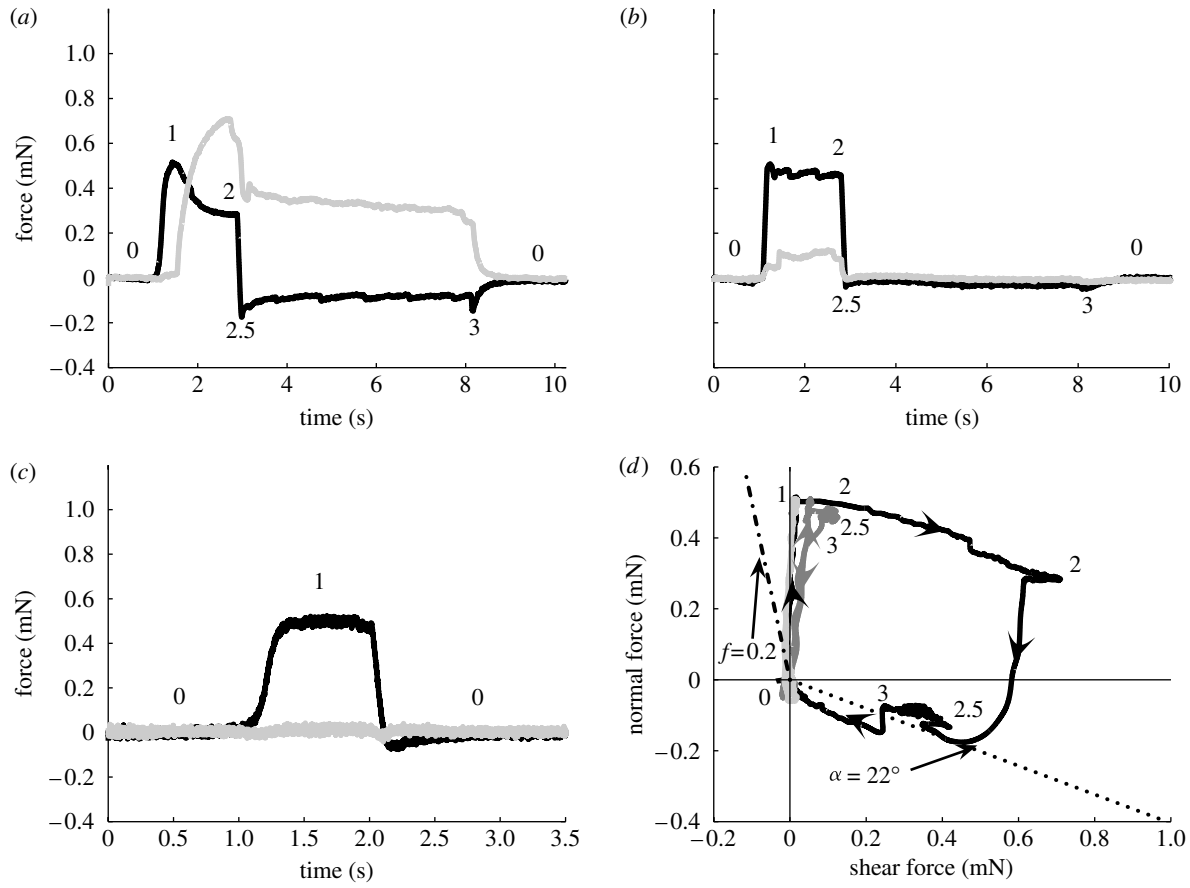

Figure 5. LDP tests with 1 μm retraction (point 2.5) on (*a*) fibrillated patch and (*b*) smooth polypropylene control. (*c*) Normal indentation and pull-off without drag (load/pull) on fibrillated patch shows minimal adhesion. (*d*) Plots (*a*–*c*) in force space demonstrate frictional adhesion. Other descriptions are similar to figure 4.

repeated shearing, an indentation experiment (load/pull; grey line in figure 8) shows zero normal pull-off force. It is seen from figure 8 that the sample's shear and tensile adhesive forces greatly increase from repeated LDP tests. This increase is possibly due to angling of the fibres (see §4; Lee *et al.* 2008). The maximum normal pull-off force and its corresponding shear force (point 3 in figure 8) for each trial is displayed in figure 9. For a given preload and sample, up to 150 tests were performed on a single area. Therefore, the trends shown in figure 9 reflect the behaviour noted in figure 8. The control, however, does not show any increase, staying centred near zero normal and shear force during pull-off. Figure 9*a*,*b* shows that the data are bounded by a range of α values observed in the various samples. These differences are due to variations in the number of tests on a given spot, and the non-uniformity of fibres (e.g. fibre length variation) across a sample. Non-uniformity of the fibres accounts for different initial angle values and then repeated tests in a particular area increase the angle.

A moderate directionality effect was observed when, after performing an LDP experiment in one direction (L→R) several times, the shear direction was reversed (R→L). For example, in L→R drags on a sample, maximum shear force at zero normal force was 1.5 mN and pull-off force was −0.2 mN. After reversing dragging direction, maximum shear force at zero normal force was 0.7 mN and pull-off force was greater than −0.1 mN.

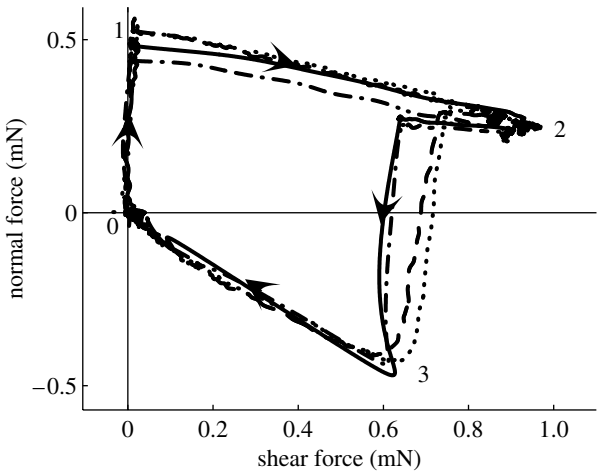

Figure 6. Normal force versus shear force for LDP experiments performed at speeds between 5 and 100 μm s^{-1}. Dashed line, 5 μm s^{-1}; dotted line, 10 μm s^{-1}; dot-dashed line, 50 μm s^{-1}; solid line, 100 μm s^{-1}.

4. DISCUSSION

To explain the results from the spherical indenter, we use a model that considers adhesive sliding of a single fibre on a sphere as well as ensemble behaviour over the contact region. This model can also be used to explain the effects of repeated loading of the fibres. A comparison of the synthetic and natural gecko fibres shows that, while the simple vertical stalks are enough

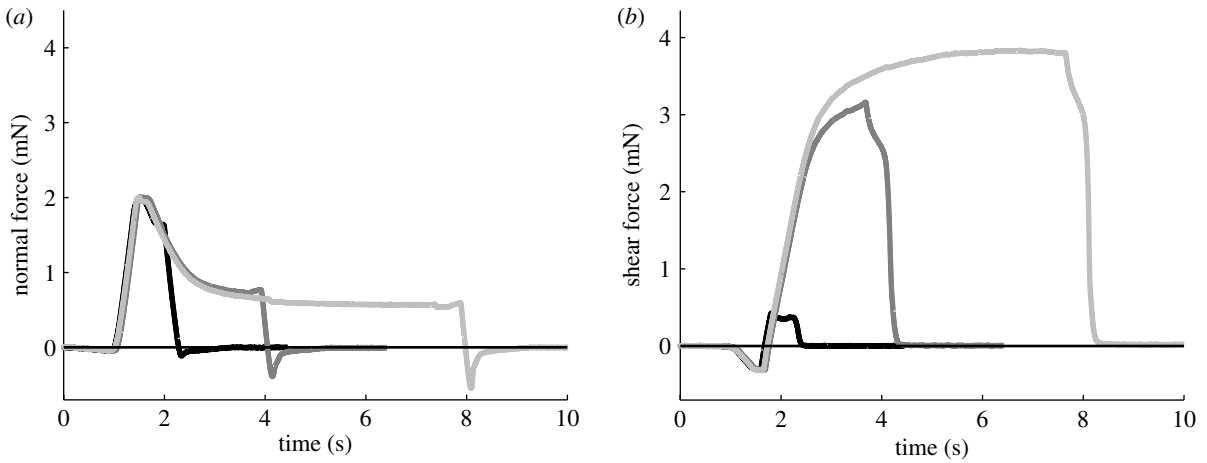

Figure 7. (*a*) Normal force and (*b*) shear force for LDP experiments performed over sliding distances of 2 µm (black line), 20 µm (dark grey line) and 60 µm (light grey line).

to achieve frictional adhesion, higher-level structures are needed to improve performance.

4.1. Frictional adhesion cantilever model

Under tension loading (the pull-off phase) with small deflections, the fibres can be treated as cantilevers (Sitti & Fearing 2003). This is in contrast to Lee *et al.* (2008), where the complete elastica solution must be considered owing to the higher loads. However, the cantilever model does not hold during the load and drag phases where fibre buckling is likely to occur.

Let stalk length and radius be l and r, respectively. For a cylindrical cantilever with modulus E, the lateral stiffness is

$$k_\theta = \frac{F_\theta}{\Delta_\theta} = \frac{3\pi r^4 E}{4l^3}. \tag{4.1}$$

With $E=1$ GPa, $r=0.3$ µm and $l=20$ µm, the lateral stiffness is 2.4 mN m^{-1}. The cantilever can be modelled as a rigid rod with a spring-loaded rotary joint at the base for small deflections (Howell 2001) as shown in figure 10. Rotation of the rod requires an applied force F_θ

$$F_\theta = k_\theta l(\theta_0 - \theta). \tag{4.2}$$

If only the tip makes contact with the sphere during pull-off, then it is assumed that sliding occurs when $F_\mathrm{t} = \pm\tau A_\mathrm{t}(F_\mathrm{n})$, where τ is the interfacial shear strength (10 MPa for polypropylene on glass; Pooley & Tabor 1972) and the tip–substrate true contact area A_t follows Johnson–Kendall–Roberts (JKR) theory[1] (Johnson *et al.* 1971):

$$A_\mathrm{t}(F_\mathrm{n}) = \pi\left\{\frac{3(1-\nu^2)R_\mathrm{t}}{4E}\left(-F_\mathrm{n} + 3\pi W_\mathrm{ad}R_\mathrm{t} + \sqrt{-6\pi F_\mathrm{n} W_\mathrm{ad}R_\mathrm{t} + (3\pi W_\mathrm{ad}R_\mathrm{t})^2}\right)\right\}^{2/3}, \tag{4.3}$$

where R_t is the tip radius; ν is Poisson's ratio; and W_ad is the work of adhesion (approx. 30 mJ m^{-2} for polypropylene on glass; Gracias & Somorjai 1998). By linearizing equation (4.3) about $F_\mathrm{n}=0$, we can express the necessary tangential force for sliding as a function of the normal load F_n:

$$\begin{aligned} F_\mathrm{t} &= \pm\tau A_\mathrm{t}(F_\mathrm{n}) \\ &\approx \pm\tau\left[A_\mathrm{t}(F_\mathrm{n}=0) + \frac{\mathrm{d}A_\mathrm{t}(F_\mathrm{n}=0)}{\mathrm{d}F_\mathrm{n}}F_\mathrm{n}\right] \\ &\approx \pm\mu(F_0 + F_\mathrm{n}), \end{aligned} \tag{4.4}$$

where $F_0 = (9/2)\pi R_\mathrm{t} W_\mathrm{ad}$ and $\mu = \tau(\mathrm{d}/\mathrm{d}F_\mathrm{n})A_\mathrm{t}(F_\mathrm{n}=0)$. Owing to the moulding fabrication process, the ends of the fibres are not hemispherical (figure 2), and probably do not make a very good contact with the sphere. To fit the experimental data, we used $R_\mathrm{t}=0.15$ µm, only half the actual fibre radius. With this contact radius, we obtain $\mu=0.2$ and $F_0=64$ nN. The JKR pull-off force for a sphere contacting a flat is $F_\mathrm{JKR} = (3/2)\pi R_\mathrm{t} W_\mathrm{ad}$ (Johnson *et al.* 1971), which gives 21 nN for our tips.

During pull-off, it can be seen from figure 10 that fibre tips are sliding to the left on the sphere, hence for quasi-static equilibrium, $F_\mathrm{t}>0$. Thus, we choose

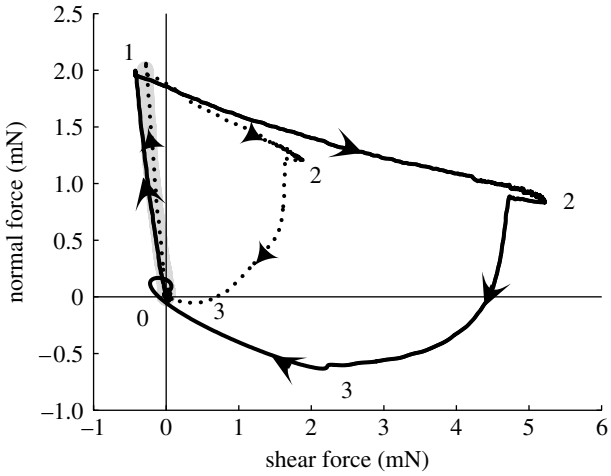

Figure 8. Normal versus shear force shows increasing frictional adhesion after 146 LDP trials in the same spot. Also shown is a load/pull experiment performed prior to LDP experiments. Numbers along curves correspond to the loading stages shown in figure 3*b*. Grey line, load/pull; dotted line, first shear test; black line, 146th shear test.

[1]The Tabor parameter (Johnson 1997) is approximately 1.6 which suggests the contact is within the DMT–JKR transition region, but it is closer to the JKR region. The difference between the DMT–JKR transition region and JKR is slight enough that we will assume JKR for simplicity.

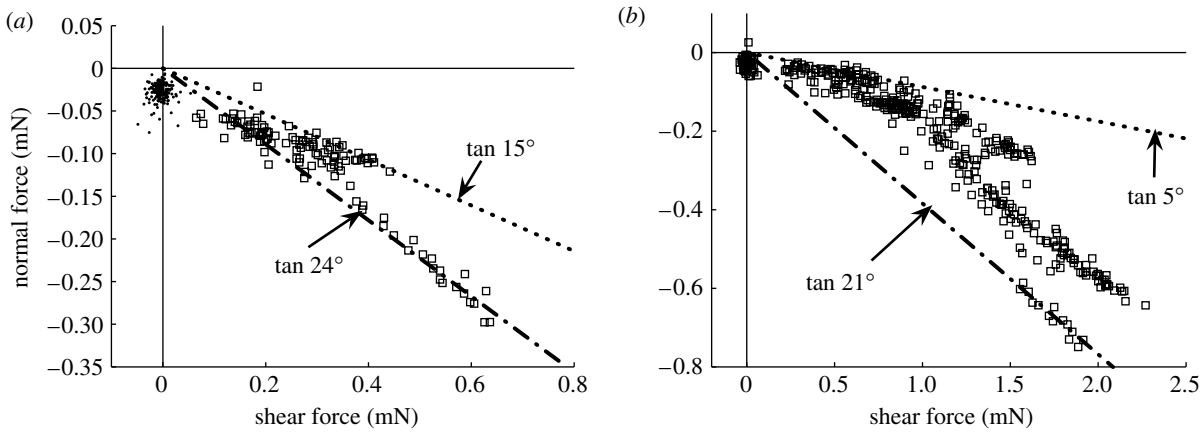

Figure 9. Data points represent the shear force measured at the highest pull-off value for LDP experiments with preloads of (*a*) 0.5 mN (squares, 117 trials for microfibre patches; dots, 182 trials for controls) and (*b*) 2.0 mN (squares, 404 trials for microfibre patches; dots, 75 trials for controls) on five microfibre patches and two smooth controls. Dashed lines represent the tangent of the critical angle of detachment, α.

the side of the 'friction cone' which corresponds to $F_t = +\mu(F_0 + F_n)$, and from Sitti & Fearing (2003), the normal force is

$$F_n(\theta) = \frac{-k_\theta l(\theta_0 - \theta) - \mu F_0 \sin\theta}{\mu \sin\theta + \cos\theta}. \qquad (4.5)$$

A related expression was derived by Tian *et al.* (2006), assuming that the lateral stiffness k_θ was negligible and the fibre was in pure tension.

The fibre tip contact location on the sphere can be calculated as the intersection of circles with radius l (the fibre length) and sphere radius R, with $\theta = f(l, R, \delta, x)$, where δ is the indentation depth and x is the location of the fibre base. During unloading, a fibre contact is maintained only for $F_n > -F_{JKR}$. Owing to fibre height variation, the actual number of contacts and hence the force will be reduced. Optical microscope examination of patches shows an approximately uniform distribution of fibre lengths from 17 to 20 μm. For a given fibre location x, we estimate effective F_n by averaging over this range of fibre lengths. Figure 11*a* shows estimated normal and shear forces under the centreline of the sphere for an indentation depth of $\delta = 4$ μm. The normal component without fibre height variation has twice the peak compressive force of the array with uniformly distributed fibre lengths. The normal force follows the expected shape, with the central region in compression and outer regions in tension. As expected for fibre tips sliding to the left during pull-off, the tangential force F_t is positive over the whole contact.

For a given indentation δ, the total normal and shear forces on the sphere are given, respectively, by

$$F_{sphere}(\delta) = \rho \int\int F_n(\theta(x, y, \delta))\mathrm{d}x\,\mathrm{d}y, \qquad (4.6)$$

$$V_{sphere}(\delta) = \rho \int\int F_t(\theta(x, y, \delta))\mathrm{d}x\,\mathrm{d}y, \qquad (4.7)$$

where $F_t = \mu(F_0 + F_n)$ for fibres in contact and 0 otherwise, and $\rho = 42 \times 10^6\ \mathrm{cm}^{-2}$ is the fibre density. The integration is performed numerically, assuming fibre height variation, and that fibre bending is restricted to the plane parallel to the probe drag direction. The predicted net normal and shear force during pull-off is shown in figure 11*b* for $\theta_0 = 70°$ and 85°.

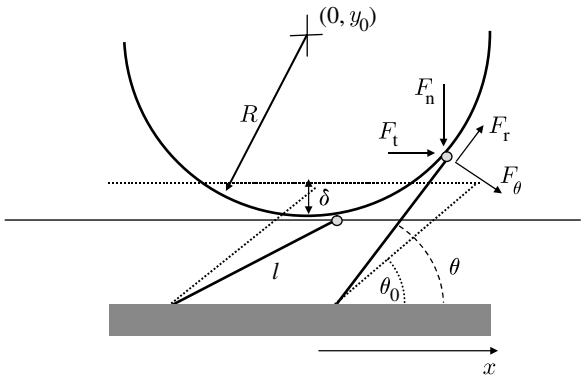

Figure 10. Cantilever model of fibres contacting spherical probe.

In addition to agreement with normal and shear force values, the cantilever model also predicts that the maximum pull-off value occurs at 2 μm indentation depth. Although at $\delta = 2$ μm fibres are still compressed ($\theta < \theta_0$), a large negative F_n is required for fibres to slide due to the adhesive component F_0. Hence, the peak normal adhesive force occurs while the sphere is indenting the surface, rather than at $\delta = 0$ as predicted by a simple vertical spring model (Schubert *et al.* 2007). Taking this into account, the force per individual fibre in the sphere pull-off test is modest (≈ 10 nN), primarily due to small R_t in tip contact as a result of tip roughness as seen in figure 2.

The data fit of figure 11*b* depends on two parameters, estimated fibre tip radius R_t and nominal fibre angle θ_0. The fibre tip radius estimate of 0.15 μm was used for both the experimental fits, and only the angle parameter was matched. The model shows good general agreement with the experiment, in particular, the coupling of shear and normal force in pull-off. The model highlights the sensitivity to initial angle θ_0. An initial angle of 45° would increase pull-off force from −0.7 to −3 mN. The results of the modelling and LDP experiments make a compelling argument for fibre angling. This angling by shearing has been observed in optical microscope images in Lee *et al.* (2008), where the shear forces per fibre are approximately 20 times higher and the contact area is greater. The much smaller shear forces generated by the spherical probe

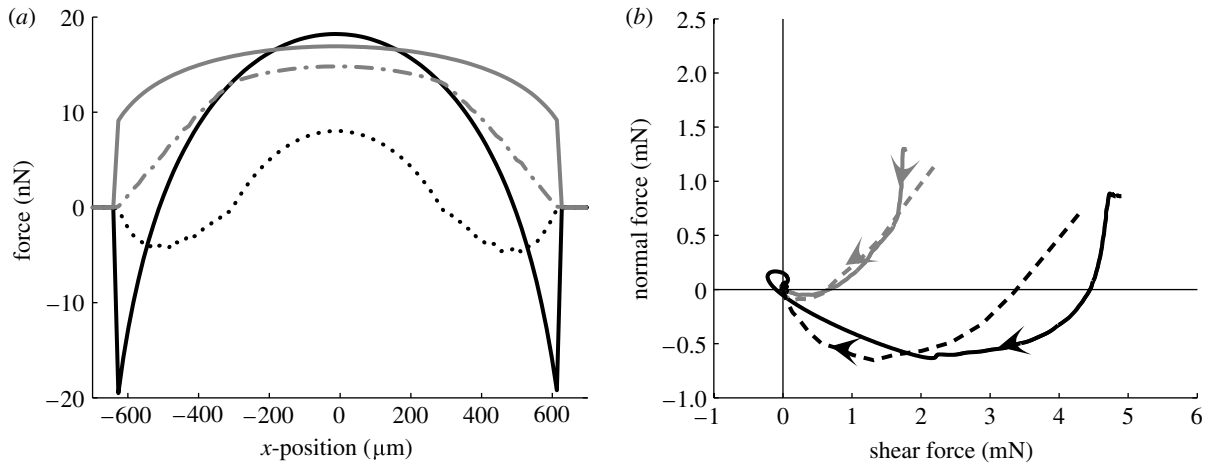

Figure 11. (*a*) Calculated normal and shear force on fibres under centreline of probe during pull-off for probe indentation 4 μm, and fibres inclined at $\theta_0=70°$ from horizontal. Fibre height variation significantly reduces normal force. Black line, F_n ($l=18.5$ μm); dotted line, F_n ($17<l<20$ μm); grey line, F_t ($l=18.5$ μm); dot-dashed line, F_t ($17<l<20$ μm). (*b*) Force space plot of predicted normal and shear forces during pull-off for fibres with rest angles of 70° and 85°, and plots of the pull-off portion of the first LDP trial and the 146th trial for a polypropylene fibre array. Grey line, first shear test; black line, 146th shear test; grey dashed line, 85° fibres; black dashed line, 70° fibres.

test make it difficult to visually observe any angling in the small contact area.

Clearly, contact with a smooth, planar surface can result in larger tensile forces than with a spherical probe, since all fibres can be in tension. It is interesting to note that even a 5 cm radius probe has significant height variation over a 0.12 cm diameter contact region, reducing maximum tensile forces on slightly angled 20 μm long fibres. The developed model for a spherical probe can also be used to predict tensile and shear contact forces for smaller spherical asperities.

4.2. Durability and improvement with use

The cantilever model predicts that increased performance with use may be attributed to angling of fibres. However, once the repeated testing stops, the fibres apparently regain their initial shape after hours of rest. This property is demonstrated in table 1 which shows the shear and normal forces measured on trials 1 and 146 (figure 8), and then values measured after the repeated shearing ceased. Over the course of 17 hours, the fibres return to their initial behaviour. It is interesting to note that Ariyama (1996) showed stress relaxation of isotactic polypropylene to steady state after 800 s, which suggests that fibres may relax to a vertical non-adhesive conformation with disuse. This property of polypropylene means that any increased performance will be lost if not constantly used. However, it also shows that the fibres are resilient and resistant to wear. The next obvious step is to create permanently angled fibres that show high performance with their first use. This could possibly be achieved with a process similar to that used by Aksak *et al.* (2007).

4.3. Natural versus synthetic geometry

As defined in equation (1.1), the interdependence of the shear force and the maximum pull-off force in the frictional adhesion model can be expressed through a critical angle α. In figure 9, the critical angle is shown to

Table 1. Shear and normal force during pull-off. (Time column refers to amount of time elapsed after repeated LDP experiments ceased. Time elapsed between trials was approx. 10 s.)

	shear (mN)	normal (mN)
trial		
1	0.24	−0.05
146	2.16	−0.63
time (*hour*)		
0.3	1.74	−0.36
2	1.64	−0.29
17	0.26	−0.01

range between approximately 15° and 24° for 0.5 mN preloads and between 5° and 21° for 2.0 mN preloads. In the gecko, the angle ranges from $\alpha=25$–30° (Autumn *et al.* 2006*b*), and soft polymer structures produce an $\alpha\approx35°$ (Santos *et al.* 2007).

A higher frictional adhesion angle corresponds to a structure that is more adhesive in the normal direction, thus it is not surprising that the soft polymer structures have the highest angle and the stiffer polypropylene fibres have the lowest. However, material stiffness is not the only indicator of frictional adhesion angle. As noted earlier, polypropylene has an elastic modulus near that of β-keratin, and yet the natural setal arrays have a higher frictional adhesion angle. This difference is due in part to the lower effective modulus of the gecko's fibre arrays. Vertical polypropylene fibres rely on shear forces to angle the fibres and generate necessary compliance, whereas setal arrays are inherently compliant as a result of natural angling and hierarchy (Autumn *et al.* 2006*a*).

The frictional adhesion angle is also influenced by the spatular tips found on the gecko's adhesive fibrils that provide greater contact area than the blunt tips of our synthetic fibres. However, side contact (Majidi *et al.* 2005; Majidi 2007) may be a possible substitution for tip structure, provided the fibres are subjected to

high shear forces, like those seen in Lee *et al.* (2008). We thus expect that hierarchy and angling, coupled with tip structure or side contact, may generate frictional adhesion angles and forces closer to the natural gecko.

5. CONCLUSION

Naturally vertical fibres produced from a material with similar stiffness to the gecko's show frictional adhesion, the same property used by geckos to scale walls. The experimental results with a spherical probe match reasonably to a cantilever model for the fibres using a JKR approximation for sliding forces. The synthetic fibres possess high durability, surviving over 100 LDP experiments with marked improvement in pull-off and shear force, and slight improvement in directionality. These gains are probably the result of temporary angling, and the patch returns to a non-adhesive mode with disuse. Processes to permanently angle fibres could be pursued to reduce training requirements. With the lightly loaded conditions tested, we estimate $\approx$10 nN tensile force per fibre from the LDP experiment at $\alpha = 22°$. In comparison, Autumn *et al.* (2000) estimated 20–200 nN tensile force per spatula (measured $\approx$20 μN per seta, and 100–1000 spatulae per seta) at $\alpha = 30°$. In order to increase the force of the polypropylene fibres, more contact at the tips needs to be generated by modifying their structure or producing enough shear to create side contact. However, achieving frictional adhesion and durability with synthetic fibre arrays already represents a significant step towards producing a true gecko-inspired adhesive that can be put to practical use.

This work was supported by NSF NIRT (no. EEC-034730). The authors wish to thank Brian Bush for SEM work, Kellar Autumn for the use of the data for figure 1; and Erik Steltz, Aaron Hoover, Nick Gravish and Stanley Baek for their helpful comments.

REFERENCES

Aksak, B., Murphy, M. & Sitti, M. 2007 Adhesion of biologically inspired vertical and angled polymer microfiber arrays. *Langmuir* **23**, 3322–3332. (doi:10.1021/la062697t)

Ariyama, T. 1996 Viscoelastic–plastic behaviour with mean strain changes in polypropylene. *J. Mater. Sci.* **31**, 8127–8131.

Autumn, K. & Hansen, W. 2006 Ultrahydrophobicity indicates a non-adhesive default state in gecko setae. *J. Comp. Physiol. A* **192**, 1205–1212. (doi:10.1007/s00359-006-0149-y)

Autumn, K., Liang, Y. A., Hsieh, S. T., Zesch, W., Chan, W.-P., Kenny, W. T., Fearing, R. & Full, R. J. 2000 Adhesive force of a single gecko foot-hair. *Nature* **405**, 681–685. (doi:10.1038/35015073)

Autumn, K., Majidi, C., Groff, R. E., Dittmore, A. & Fearing, R. S. 2006*a* Effective elastic modulus of isolated gecko setal arrays. *J. Exp. Biol.* **209**, 3558–3568. (doi:10.1242/jeb.02469)

Autumn, K., Dittmore, A., Santos, D., Spenko, M. & Cutkosky, M. 2006*b* Frictional adhesion: a new angle on gecko attachment. *J. Exp. Biol.* **209**, 3569–3579. (doi:10.1242/jeb.02486)

Gao, H. J., Wang, X., Yao, H. M., Gorb, S. & Arzt, E. 2005 Mechanics of hierarchical adhesion structures of geckos. *Mech. Mater.* **37**, 275–285. (doi:10.1016/j.mechmat.2004.03.008)

Gracias, D. H. & Somorjai, G. A. 1998 Continuum force microscopy study of the elastic modulus, hardness and friction of polyethylene and polypropylene surfaces. *Macromolecules* **31**, 1269–1276. (doi:10.1021/ma970683b)

Gravish, N., Wilkinson, M. & Autumn, K. 2008 Frictional and elastic energy in gecko adhesive detachment. *J. R. Soc. Interface* **5**, 339–348. (doi:10.1098/rsif.2007.1077)

Howell, L. L. 2001 *Compliant mechanisms*. New York, NY: Wiley.

Johnson, K. L. 1997 Adhesion and friction between a smooth elastic spherical asperity and a plane surface. *Proc. R. Soc. A* **453**, 163–179. (doi:10.1098/rspa.1997.0010)

Johnson, K. L., Kendall, K. & Roberts, A. D. 1971 Surface energy and the contact of elastic solids. *Proc. R. Soc. A* **324**, 301–313. (doi:10.1098/rspa.1971.0141)

Lee, J., Majidi, C., Schubert, B. & Fearing, R. S. 2008 Sliding-induced adhesion of stiff polymer microfibre arrays. I. Macroscale behaviour. *J. R. Soc. Interface* **5**, 835–844. (doi:10.1098/rsif.2007.1308)

Majidi, C. 2007 Remarks on formulating an adhesion problem using Euler's elastica. *Mech. Res. Commun.* **34**, 85–90. (doi:10.1016/j.mechrescom.2006.06.007)

Majidi, C., Groff, R. E. & Fearing, R. S. 2005 Attachment of fiber array adhesive through side contact. *J. Appl. Phys.* **98**, 103521. (doi:10.1063/1.2128697)

Majidi, C. *et al.* 2006 High friction from a stiff polymer using micro-fiber arrays. *Phys. Rev. Lett.* **97**, 076103. (doi:10.1103/PhysRevLett.97.076103)

Murphy, M., Aksak, B. & Sitti, M. 2007 Adhesion and anisotropic friction enhancement of angled heterogeneous micro-fiber arrays with spherical and spatula tips. *J. Adhes. Sci. Tech.* **21**, 1281–1296. (doi:10.1163/156856107782328380)

Peattie, A. M., Majidi, C., Corder, A. & Full, R. J. 2007 Ancestrally high elastic modulus of gecko setal β-keratin. *J. R. Soc. Interface* **4**, 1071–1076. (doi:10.1098/rsif.2007.0226)

Pooley, C. M. & Tabor, D. 1972 Friction and molecular structure: the behaviour of some thermoplastics. *Proc. R. Soc. A* **329**, 251–274. (doi:10.1098/rspa.1972.0112)

Santos, D., Kim, S., Spenko, M., Parness, A. & Cutkosky, M. 2007 Directional adhesive structures for controlled climbing on smooth vertical surfaces. In *Proc. IEEE Int. Conf. on Robotics and Automation, Rome, Italy, 10–14 April 2007*, pp. 1262–1267.

Schubert, B., Majidi, C., Groff, R. E., Baek, S., Bush, B., Maboudian, R. & Fearing, R. S. 2007 Towards friction and adhesion from high modulus microfiber arrays. *J. Adhes. Sci. Tech.* **21**, 1297–1315. (doi:10.1163/156856107782328344)

Sitti, M. & Fearing, R. S. 2003 Synthetic gecko foot-hair micro/nano-structures as dry adhesives. *J. Adhes. Sci. Tech.* **18**, 1055–1074. (doi:10.1163/156856103322113788)

Spolenak, R., Gorb, S. & Arzt, E. 2005 Adhesion design maps for bio-inspired attachment systems. *Acta Biomater.* **1**, 5–13. (doi:10.1016/j.actbio.2004.08.004)

Tian, Y., Pesika, N., Zeng, H., Rosenberg, K., Zhao, B., McGuiggan, P., Autumn, K. & Israelachvili, J. 2006 Adhesion and friction in gecko toe attachment and detachment. *Proc. Natl Acad. Sci. USA* **103**, 19 320–19 325. (doi:10.1073/pnas.0608841103)

Varenberg, M. & Gorb, S. 2007 Shearing of fibrillar adhesive microstructure: friction and shear-related changes in pull-off force. *J. R. Soc. Interface* **4**, 721–725. (doi:10.1098/rsif.2007.0222)